Mass Transfer Limited KOH Etching in Crystalline Silicon using a Confinement Mask

ECS Journal of Solid State Science and Technology, 2020 **9** 034013
2162-8777/2020/9(3)/034013/8/$40.00 © 2020 The Electrochemical Society ("ECS"). Published on behalf of ECS by IOP Publishing Limited

Mass Transfer Limited KOH Etching in Crystalline Silicon using a Confinement Mask

Kristianto Tjiptowidjojo,[1,2,z] Seok Jun Han,[2] Sang Eon Han,[2] Sang M. Han,[2] and P. Randall Schunk[1,2,3]

[1]*Center for Micro-Engineered Materials, University of New Mexico, Albuquerque, New Mexico 87131-0001, United States of America*
[2]*Department of Chemical and Biological Engineering, University of New Mexico, Albuquerque, New Mexico 87131-0001, United States of America*
[3]*Sandia National Laboratories, Albuquerque, New Mexico 87185-0826, United States of America*

We demonstrate the use of a confinement mask to control the etch depth gradient in nanopatterned crystalline silicon. The gradient is set by controlling the clearance gap of the mask. We also develop a wafer-scale model that accounts for etchant transport, flow, and surface reaction in order to predict etch depth profiles for two different masks. Results from the model reveal that the gradient is best achieved by varying the clearance between nanometer and micrometer scale in a periodic fashion. The results are qualitatively validated with experimental demonstration and observation.
 [DOI: 10.1149/2162-8777/ab8063]

Manuscript submitted November 7, 2019; revised manuscript received March 13, 2020. Published April 1, 2020.

Solar energy production has increased steadily in recent years, especially in the residential sector.[1] However, barriers remain in installation and material cost. In the case of crystalline silicon (c-Si) solar cells, the material cost comprises as high 30–40 percent of the total cost.[2] Typical bulk c-Si panels use 130–300 μm thick wafers and require a sturdy support such as glass which contributes to a higher cost of installation due to weight. Using thinner c-Si films (less than 50 μm) would reduce material and installation costs as they can be supported with a light-weight polymer-based substrate. However thinner c-Si films reduce light absorption and thereby decrease photovoltaic efficiency of the panel. One viable approach to enhance light trapping is to engineer topological nanostructures on the c-Si cell surface.

Various light trapping schemes have been studied, including metal nanoparticles,[3] nanowires/nanoholes,[4,5] random corrugation,[6,7] and periodic diffraction gratings.[8–11] Metal nanoparticles can enhance absorption in a photoactive film by efficiently scattering light into it. However, the particles themselves typically absorb significant fraction of incident light. Nanowires/nanoholes can also increase absorption, but their large surface area tends to increase charge carrier recombination. Random corrugation is currently the most cost-effective and widely used scheme in commercial solar cells. However, the random nature of the structures makes it difficult to control and optimize the optical and electrical properties. In comparison, periodic diffraction gratings enable systematic optimization and control of these properties. Though fabrication of the periodic structures increases the manufacturing cost, the advantages of the efficiency enhancement and the evenness in product quality that come from precise control of the structures, are crucial for future improvement of solar photovoltaics.

One efficient light trapping structure using periodic diffraction gratings in c-Si photovoltaics is inverted nano-pyramid arrays, which are the focus of our study.[9,10] However, manufacturing nano-pyramids arrays over a large area of wafers is challenging due large number of uniform features needed. For example, a periodicity of several hundreds of nanometer amounts to $\sim 1.8 \times 10^{10}$ uniform features over a 6 inch wafer. One route to a scalable manufacturing process to pattern c-Si surfaces is illustrated in Fig. 1. First, a surface of a [100] c-Si wafer is patterned with a lithography method, such as interference lithography,[12,13] that results in a 100 nm thick silicon oxide mask with $\sim$350 nm wide holes with 700 nm pitch. The c-Si [100] plane exposed by holes is then etched away in KOH solution.[14] The etching in turn exposes other crystalline planes, such as the [111], which are etched at a much slower rate due to anisotropicity of the reaction.[15] After the [100] plane under the holes is completely etched away, the resulting nanostructure takes on the form of inverted nanopyramids with a periodicity of 700 nm. Further improvement in the light-trapping capability can be realized by introducing a second periodicity by etch depth gradient to the inverted nano-pyramids, as shown by Hassan et al.[16] Such double-periodic structures would have wide applications in meta-surface photonics.[17] The second periodicity is introduced in the wet etching step as shown in Fig. 2. The left part of the figure shows the patterning of the 700 nm periodic nanopyramids outlined in previous paragraph. The right shows fabrication of a confinement mask with a 250 μm pitch as a mean to introduce the second periodicity. Here we consider two configurations of the confinement masks, labeled as masks 1 and 2, as shown in Figs. 3b and 3c. Mask 1 has 100 nm clearance on the 50 μm circular regions and 7 μm on the rest. Mask 2 has the opposite clearance profile, viz. 7 μm on the circles and 100 nm on the rest. The purpose of the confinement is to limit the rate of etchant and by-product transport such that a concentration gradient forms along the exposed c-Si surface which can lead to periodic variation of etch depth. Determining optimum confinement mask and etch conditions to enable the desired etch depth gradients can be aided by the predictive wafer-scale model that we develop in this study.

Prior modeling efforts of wet etching processes mostly focus on predicting the pattern of flow and species transport at a single feature level.[18,19] To the author's knowledge, no modeling work has been reported that accounts for multiple features or at the wafer-scale due to prohibitive computational cost. Our approach to enable wafer-scale simulation is to use a reduced-order model described in Wafer Scale Development . The model is used to predict etch depth under two confinement masks and with different orientation with respect to gravity. The results are reported in Resulrs and Discussion and their comparison to the experimental work are covered in Comparison with Experiment.

Wafer Scale Model Development

The model aims to capture species transport and reaction at disparate length scales set forth by the vertical and lateral dimensions. The wafer area addressed in this work is 0.4 cm $\times$ 0.4 cm, as shown in Fig. 4, which is three orders of magnitude larger than the clearances of both masks 1 and 2. Disparate length scales also occur in the lateral direction due to dual periodicity of the nano-patterned c-Si and the confinement masks viz. inverted nano-pyramids with 700 nm pitch vs clearance profile with 250 μm. Within each nanopyramid, the rate of mass transport is much faster than the

[z]E-mail: tjiptowi@unm.edu

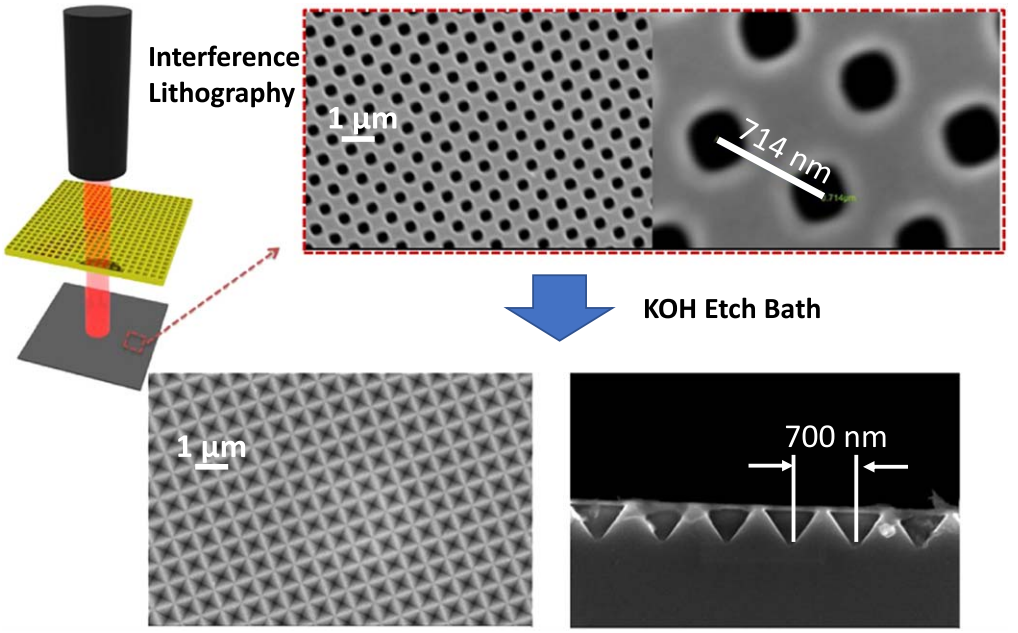

Figure 1. Fabrication of crystalline silicon with 700-nm pitch inverse nanopyramids.

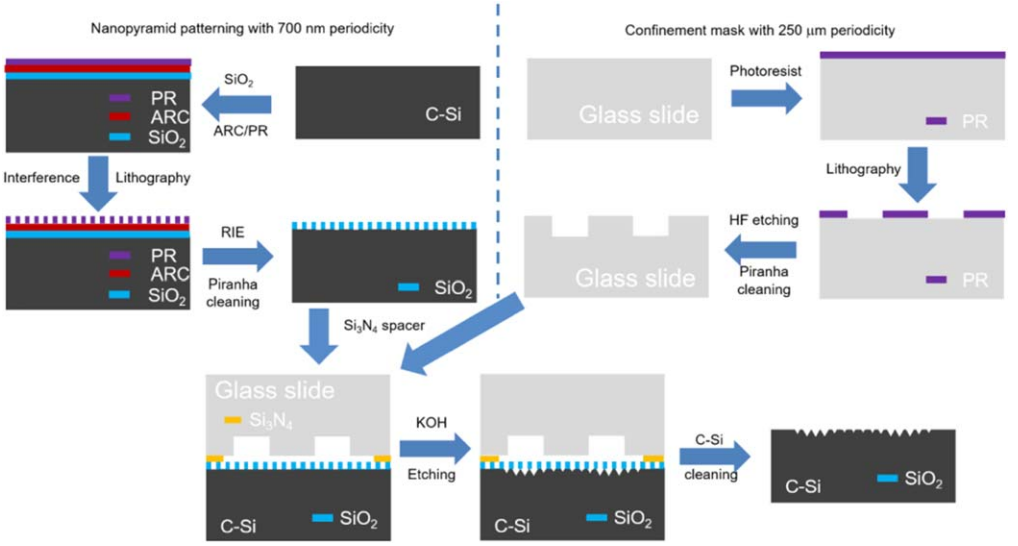

Figure 2. A process flow for fabricating a double periodicity structure in c-Si wafer using a physical mask for transported limited KOH etching.

rate of reaction. Specifically, the etching rate is several orders of magnitude slower than the diffusion rate, viz. μm per hour[15] vs mm per second. Therefore the concentration within the nano-pyramid can be considered well-mixed at any instance without loss of accuracy, even with confined flow. The disparate length scales between the vertical and lateral direction also necessitates the thin-film approximation such that the species conservation equation can be averaged along the vertical direction, which can stated mathematically as follows:

$$h\frac{\partial \rho_i}{\partial t} + \mathbf{v}_{\text{II}} \cdot (h\nabla_{\text{II}}\rho_i) = D_i \nabla_{\text{II}} \cdot (h\nabla_{\text{II}}\rho_i) + j_i. \qquad [1]$$

h is the spatially varying clearance between c-Si and confinement mask, ρ_i is mass concentration of species i per unit volume, $\mathbf{v}_{\text{II}}$ is mass-averaged liquid lateral convective velocity, ∇_{II} is gradient in lateral direction, D_i is Fickian diffusivity, and j_i is in-flux/out-flux due to etching reaction at the wafer. Seidel et al.[15] proposed the overall surface reaction as:

$$Si + 2OH^- + 2H_2O \rightarrow 2H_2 + SiO_2(OH)^{--} \qquad [2]$$

Our model only tracks species concentrations in the liquid phase, i.e. KOH, H_2O, H_2, and $SiO_2(OH)^{--}$. The rate of reaction R depends on the local surface orientation and concentration. At plane (100), its expression is given by:

$$R_{100} = k_0[H_2O]^4[OH^-]^{\frac{1}{4}} \exp\left(\frac{-E_a}{kT}\right). \qquad [3]$$

$[H_2O]$ and $[OH^-]$ are molar concentration of water and KOH, k is Boltzmann constant, and T is temperature. Rate constant k_0 and activation energy E_a values for (100) plane are reported by Seidel et al.[15] to be 2480 $(\mu\text{m/hour})(\text{mole/liter})^{-4.25}$ and 0.595 eV respectively. The etching reaction rate at plane (111) is insensitive to local concentration[20] and considered to be a function of temperature only. Within a unit cell shown in bottom of Figs. 3b and 3c, only half of the silicon surface is available for etching reaction due to the silica

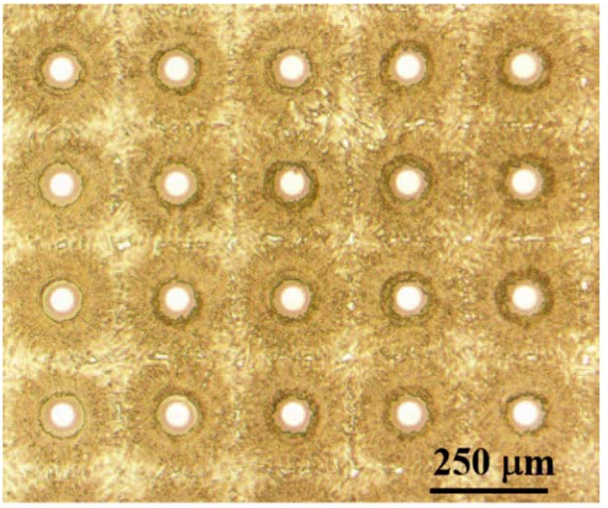

(a) Photograph of a confinement mask

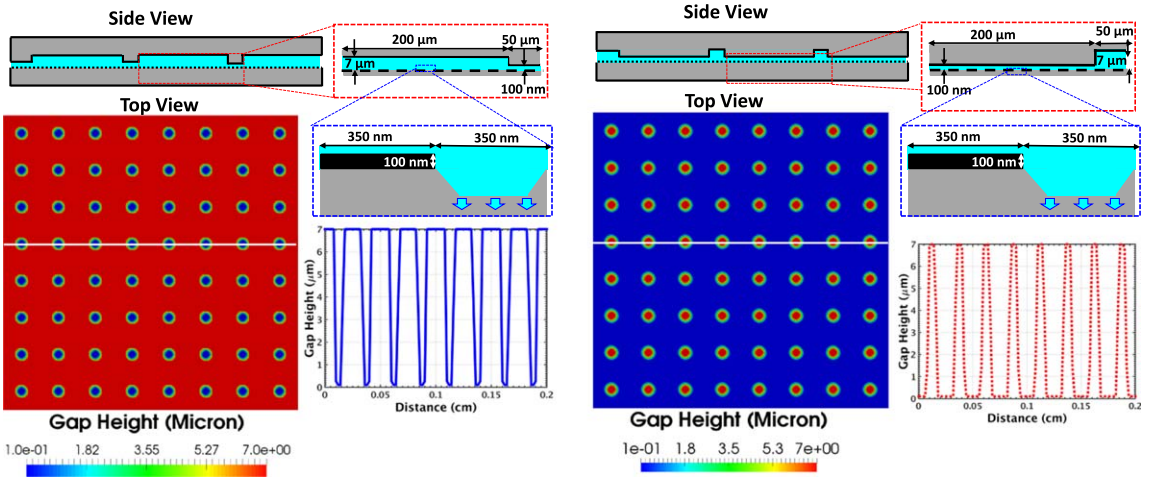

(b) Clearance profile of mask 1 with periodicity of confinement mask and c-Si highlighted

(c) Clearance profile of mask 2 with periodicity of confinement mask and c-Si highlighted

Figure 3. Confinement masks detailed features.

coverage introduced after interference lithography patterning. As etching progresses, that fraction decreases over time to form the inverted nano-pyramid. Our approach is to average the reaction rate over the whole unit cell by multiplying the rate R with the available area fraction ϕ:

$$R_{\text{avg}} = R\varphi \qquad [4]$$

The area fraction ϕ evolves with the extent of etch because of the geometric relationship between etch depth and the remaining c-Si surface. For the (100) plane, area fraction is governed by:

$$\varphi(t) = \varphi_0 - \frac{1}{\sqrt{2A_0}} \int_0^t R_{100}(t')\mathrm{d}t' \qquad [5]$$

φ_0 is the initial area fraction available over the unit cell, which in this case is 0.5, and A_0 is initial c-Si area exposed to the etchant within the unit cell, which corresponds to an area of circle with radius of 175 nm. The average etch rate R_{avg}, which is given in the units of length per time, can be related to the mass flux of silicon j_{Si} by multiplying it with its bulk density ρ_{Si}, i.e.

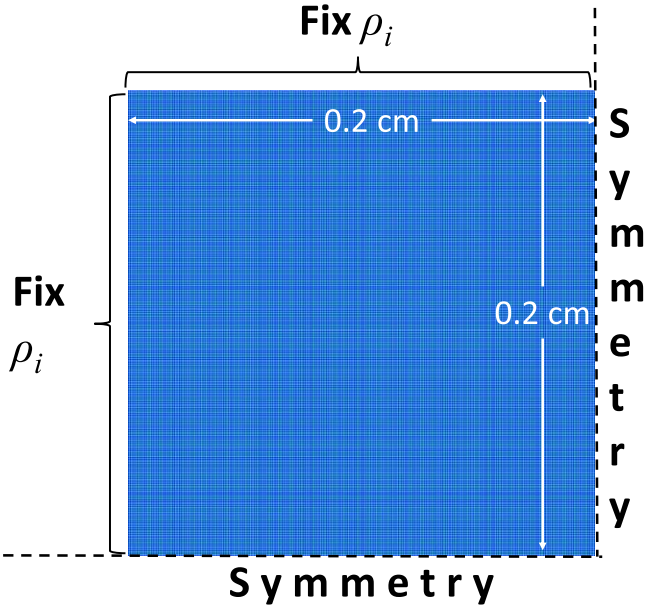

Figure 4. Model geometry and boundary conditions.

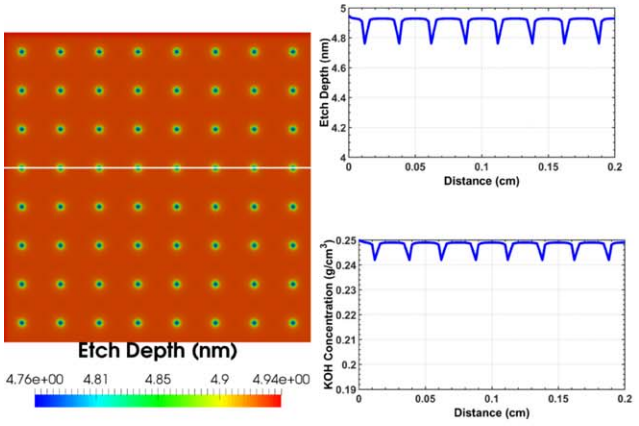

(a) Etch depth and KOH concentration profile at $t =$ 1 s of mask 1

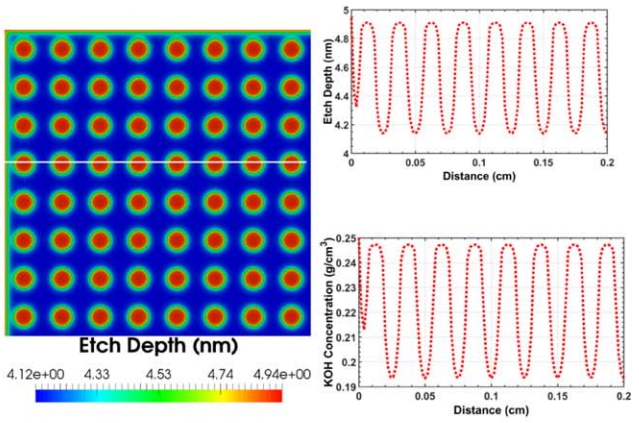

(b) Etch depth and KOH concentration profile at $t =$ 1 s of mask 2

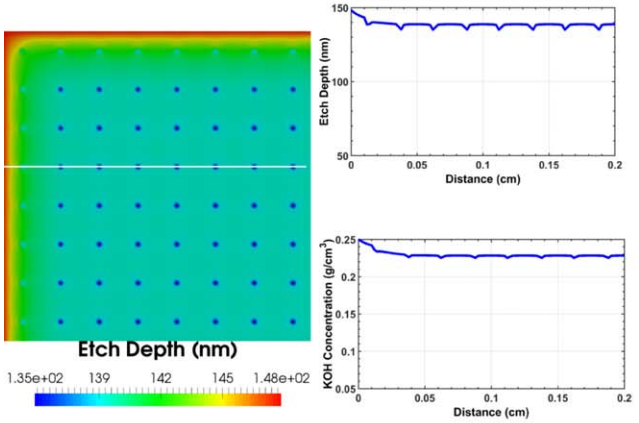

(c) Etch depth and KOH concentration profile at $t =$ 30 s of mask 1

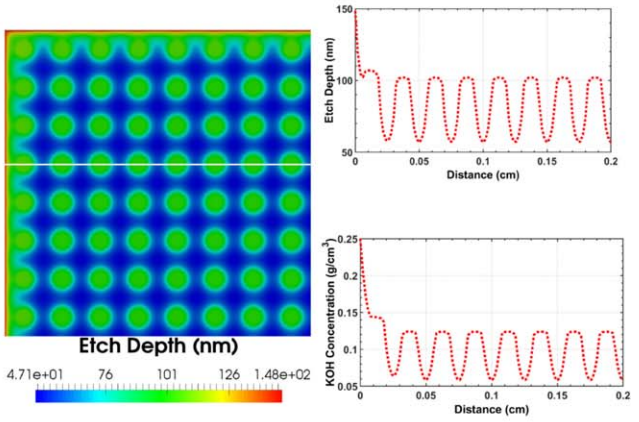

(d) Etch depth and KOH concentration profile at $t =$ 30 s of mask 2

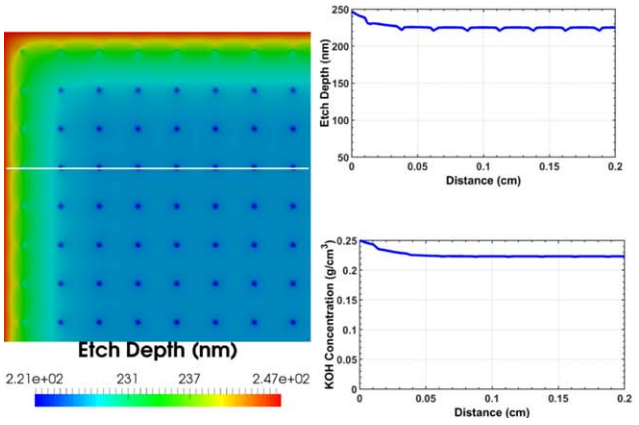

(e) Etch depth and KOH concentration profile at $t =$ 50 s of mask 1

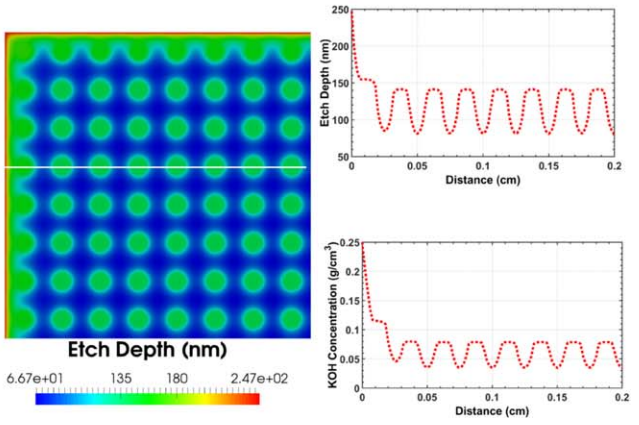

(f) Etch depth and KOH concentration profile at $t =$ 50 s of mask 2

Figure 5. Comparisons of etch depth and KOH concentration profiles between masks 1 and 2. Etch depth is expressed in nm and the KOH concentration in terms of mass per volume with unit of g cm^{-3}. Mask 2 with its higher density of 100-nm-clearance regions present heightened mass transfer limitation in etchant supply from the bath leading to more disparate etch depth profile compared to Mask 1 in which its etch depth variation is negligible.

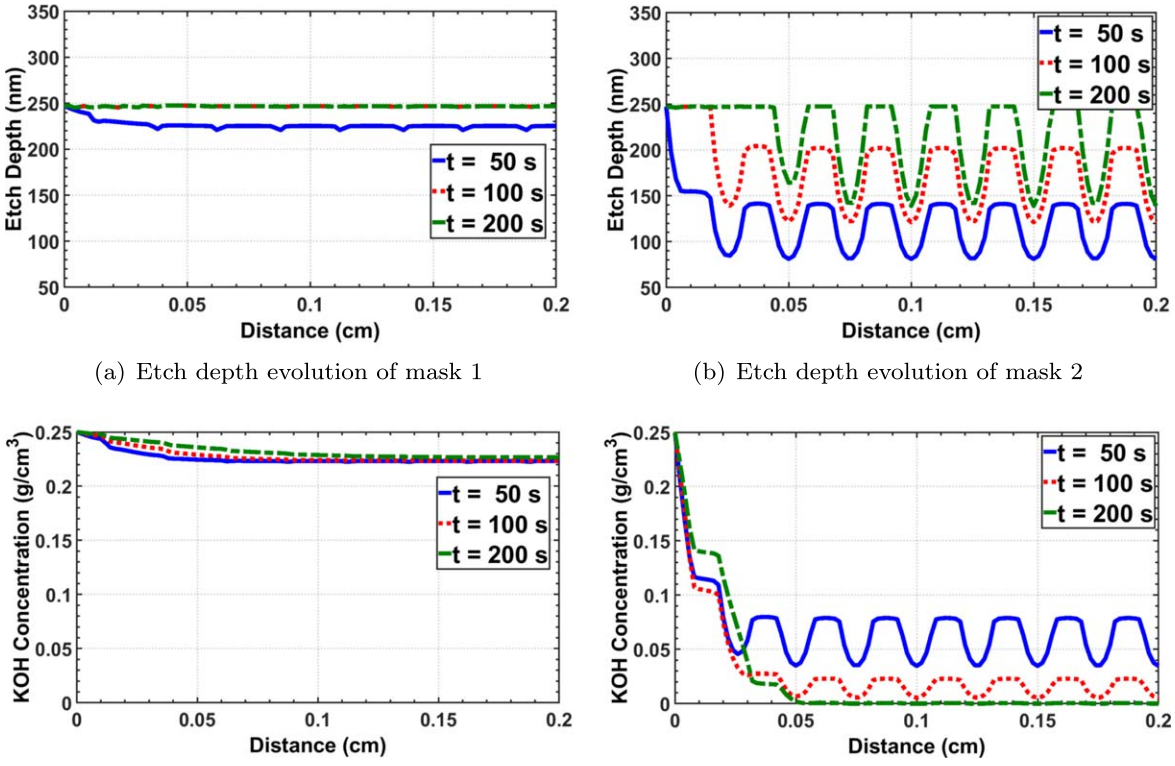

(a) Etch depth evolution of mask 1

(b) Etch depth evolution of mask 2

(c) KOH concentration evolution of mask 1

(d) KOH concentration evolution of mask 2

Figure 6. Etch depth and KOH concentration profile evolution. Etch depth is expressed in nm and the KOH concentration in terms of mass per volume with unit of g cm^{-3}. At $t = 50$ s and longer, KOH concentration in mask 2 is mostly depleted leading to shallower etch depth especially in the 100-nm regions. In contrast, mass transfer limitation does not persist which leads to a uniform etch depth.

$$j_{Si} = R_{\text{avg}}\rho_{Si}$$

Fluxes of other species can be computed using stochiometric coefficients according to the reaction, Eq. 2, and their molecular weights M_i:

$$j_{OH^-} = 2\frac{M_{OH^-}}{M_{Si}}j_{Si} \quad [6]$$

$$j_{H_2O} = 2\frac{M_{H_2O}}{M_{Si}}j_{Si} \quad [7]$$

$$j_{SiO_2(OH)^{--}} = -1\frac{M_{SiO_2(OH)^{--}}}{M_{Si}}j_{Si} \quad [8]$$

$$j_{H_2} = -2\frac{M_{H_2}}{M_{Si}}j_{Si} \quad [9]$$

The convective velocity, $\mathbf{v}_{\text{II}}$, results from the flow driven by buoyancy force due to lateral concentration gradient (and hence density gradient). In accordance to thin gap approximation, we use the Reynolds lubrication equation to describe the flow field[21]:

$$h\frac{\partial\rho}{\partial t} + \nabla_{\text{II}}\cdot(h\mathbf{v}_{\text{II}}) + J = 0 \quad [10]$$

$$\mathbf{v}_{\text{II}} = \frac{h^2}{12\mu}(-\nabla_{\text{II}}p + \rho\mathbf{g}) \quad [11]$$

Here, $\rho = \sum_{i=1}^{N} C_i$ is total mass concentration, J is net total mass out-flux due to surface etching reaction, μ is liquid viscosity, p is pressure, and $\mathbf{g}$ is gravitational acceleration. As shown in Eq. 11, the lateral gradient of species concentration C_i, hence the associated density gradient, drives the convection flow as long the gravitational acceleration $\mathbf{g}$ is not perpendicular to the nano-patterned c-Si surface.

Boundary conditions for the species conservation Eq. 1 are as follows: At the opening to the etch bath, which is located at the left and top edges in Fig. 4, we assume that the solution is well mixed and the etchant byproducts are dispersed away such that the concentration of each species is fixed. Symmetry conditions are enforced at other boundaries, i.e. no net flux of each species is permitted. The lubrication flow Eq. 10 requires boundary conditions on pressure. We set the pressure to atmospheric when the direction of gravity is perpendicular to the nano-patterned c-Si surface. In other cases, the pressure values are adjusted accordingly.

The equations above are solved with Goma 6.0,[22] an open-source finite element software originally developed by Sandia National Laboratories. Simulation results are discussed next.

Results and Discussion

First we performed simulations with the c-Si surface oriented perpendicular to the direction of gravity such that buoyancy driven flow does not play a role in the lateral transport. The etch bath concentration is set to at 20% KOH solution. A comparison of etch depth and KOH concentration between masks 1 and 2 at different times is shown in Fig. 5.

After 50 s, the outer edges form complete nano-pyramids with etch depth of 247 nm due to fixed solute boundary condition there. In the interior, at a distance greater than 0.5 mm from the edges, the etch depth varies in periodic fashion corresponding to the clearance profile of the masks. Regions with 7 μm clearances have deeper etch than that of 100 nm, but the difference is more pronounced in mask 2. This indicates that the etch depth in the interior is controlled

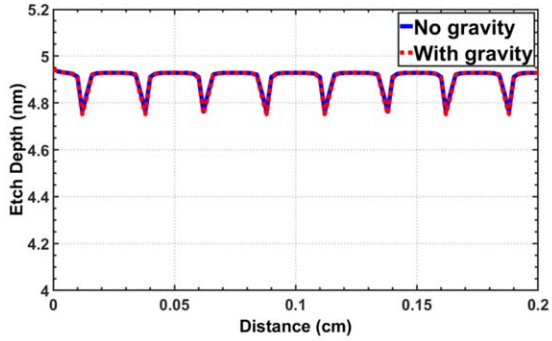

(a) Etch depth profile comparison at $t = 1$ s of mask 1

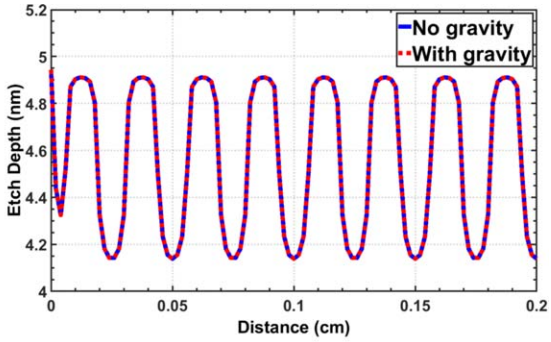

(b) Etch depth profile comparison at $t = 1$ s of mask 2

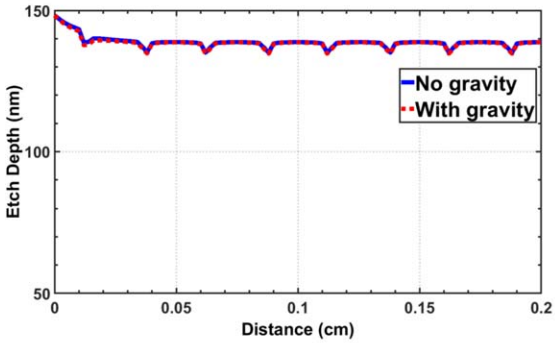

(c) Etch depth profile comparison at $t = 30$ s of mask 1

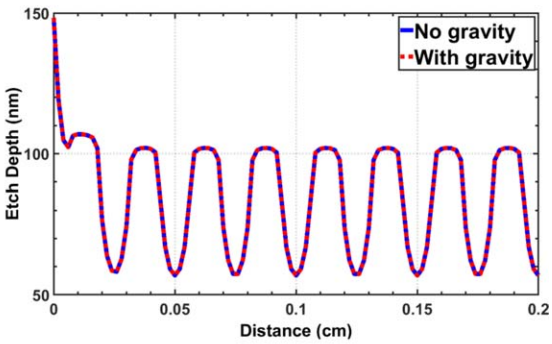

(d) Etch depth profile comparison at $t = 30$ s of mask 2

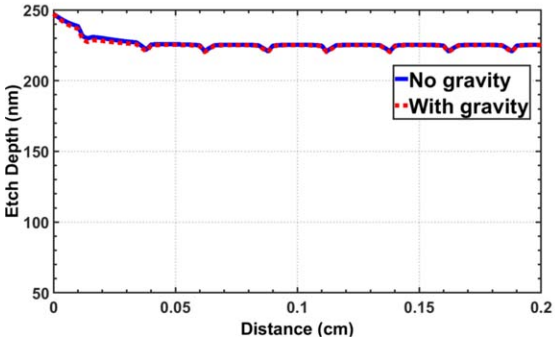

(e) Etch depth profile comparison at $t = 50$ s of mask 1

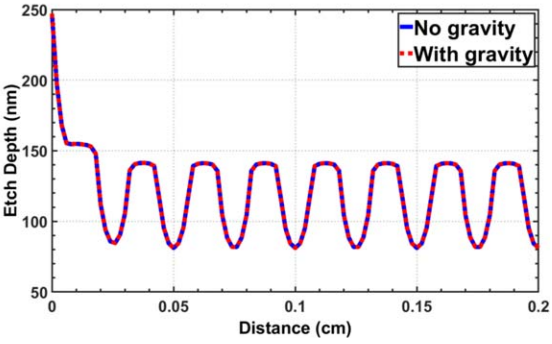

(f) Etch depth profile comparison at $t = 50$ s of mask 2

Figure 7. Etch depth profile comparisons between horizontal and vertical orientations. Etch depth is expressed in nm and the KOH concentration in terms of mass per volume with unit of g/cm^3. The effect of mask orientation with respect to gravity does not lead to significant differences in etch profile for masks 1 and 2, which suggest that the buoyancy flow induced by density gradient is unimportant in the operating conditions studied.

primarily by the inventory of limiting reactant, which is KOH in this case. Mask 2 results in greater area fraction of 100 nm gap and therefore lower initial volume of KOH than mask 1. As etching progresses past 50 s, more than 80% of KOH in 100 nm regions is consumed and the etch rate is slowed down, leading to a shallower etch. Mass transfer from neighboring 7 μm regions help alleviate the KOH depletion, but not significantly. Additionally, a small gap in the 100 nm regions hinders KOH transport.

The contrast of etch depths with mask 2 persists at longer etching times, i.e. t = 200 s, and complete inverted nano-pyramids are formed in 7 μm regions together with shallow or incomplete nano-pyramids at the 100 nm region as shown in Fig. 6b. In the same time frame, KOH concentration is depleted to near zero, especially in the 100-nm regions, leading to persistent incomplete nano-pyramids. In contrast, etch depth with mask 1 becomes more uniform at longer etch time as the diffusion barrier of KOH is much lower which leads to uniform KOH distribution away from the edge. These two trends indicate that etching with mask 1 occurs in reaction-limited regime and with mask 2 in transport-limited regime.

One possibility to slow down the diffusion further is to induce buoyancy-driven flow in opposite direction. This effect is examined by performing simulations of etching in orientations such that the direction of gravity is parallel with the c-Si nanopatterned surface. The calculated etch depths at different times are compared with results in Figs. 5 and 6, as shown in Fig. 7.

Etching with mask 2 is not affected by the orientation of gravity due to the predominantly small clearance. That is, the resistance of lubrication flow is proportional to the clearance height to the third power, hence the buoyancy driven flow induced by local concentration gradient is suppressed. On mask 1, the effect of gravity is only observed near the boundaries where the concentration difference and the clearance height are the largest. This indicates that the effect of

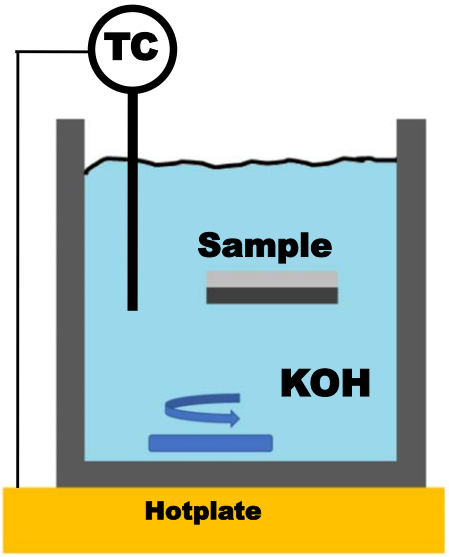

(a) Schematic of experimental setup. The sample and etch-mask are stacked by Teflon tweezers and positioned in the middle of the etch bath container.

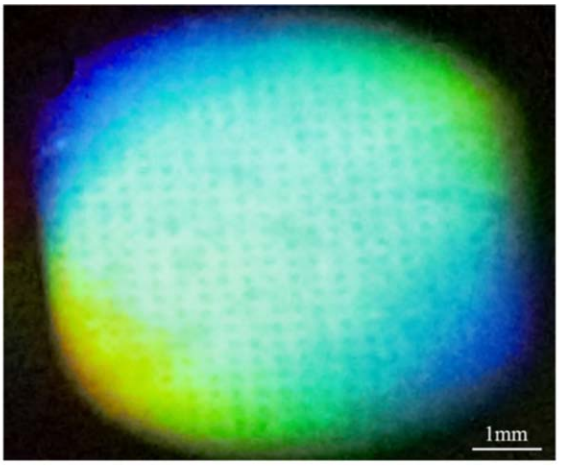

(b) Optical image of the nanopatterned c-Si

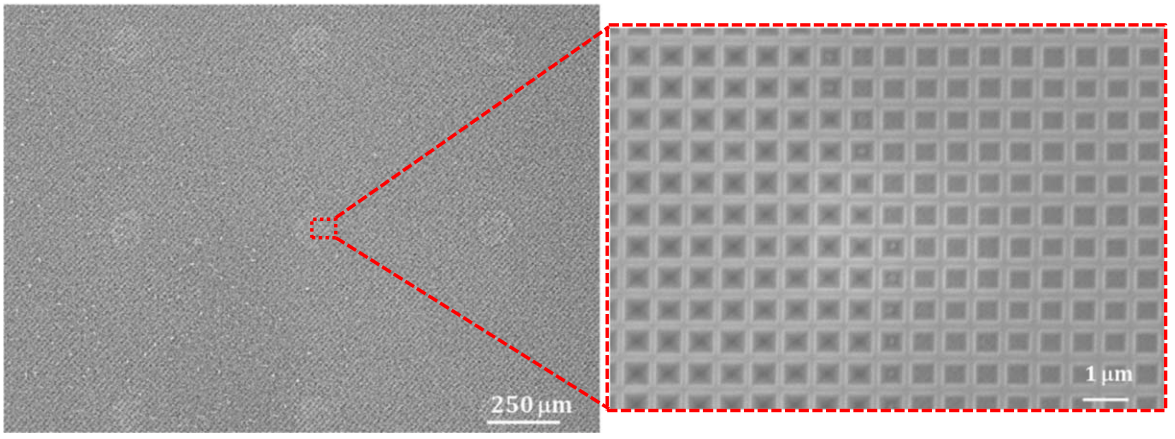

(c) SEM images of a double periodicity inverted nanopyramid array

Figure 8. Schematic of experimental setup and the resulting patterned c-Si using KOH etch bath in a confinement mask.

gravity is negligible in controlling etch depth gradient. Varying clearance profiles and their average spacing is far more effective at controlling etch-depth gradients.

Comparison with Experiment

The computer simulations show that the KOH wet etch rate of c-Si can be limited by transport of reactants and byproducts when etching is performed within a limited volume defined by a confinement mask. Because the dimension of patterns in the confinement mask is much larger than that of nanostructure, various shapes of patterns can be clearly defined by conventional lithography. An advantage of our approach is that we can separately design independently the nano-structures in a c-Si layer and the macro-structures in a confinement mask. For example, we can easily change symmetry of an inverted nano-pyramid array with double periodicity by independently rotating a KOH wet etch mask on a c-Si layer.[8] In addition to this, the fabricated confinement mask can be combined with various orientations with respect to the c-Si layer. Also, the confinement mask can be slanted on the c-Si using two different thicknesses of spacer layers on edges, and this method can introduce a gradual change in nanostructure.

As a demonstration of our approach, we fabricated double-periodicity, inverted nano-pyramid structures using a confinement mask with gap clearance profiles of mask 2. A fabrication process flow is shown in Fig. 2. The confinement mask was patterned on an inexpensive glass slide with lithography. The pattern is a square lattice of 50 μm diameter holes with 250 μm periodicity. Then, regions not covered by photoresist (PR) were etched by HF, and the depth of circular grooves was about 7 μm. The magnified image of the fabricated confinement mask is shown in Fig. 3a. The use of glass slide is not ideal for large area fabrication due to its surface roughness being comparable to the confinement mask gap. However for C-Si wafer used in the experiment, which is in the order of milimeters, the non-uniformity introduced by the glass slide does not appear to affect the nanopattern significantly.

To make a nano-pattern on a c-Si wafer, we deposited a silicon oxide (SiO_2) layer on a c-Si wafer by plasma-enhanced chemical vapor deposition (PECVD) as a mask for potassium hydroxide (KOH) etching. We sequentially spin-coated a 160-nm-thick

anti-reflection (ARC iCON-16, Brewer Science) layer and a 500-nm-thick negative photoresist (NR7-500P, Futurrex) film on SiO_2/c-Si for interference lithography. We used Lloyd's mirror interferometry with 355-nm-wavelength-light (YAG-Nd laser, Infinity 40–100, Coherent Inc..) to pattern the prepared substrate (PR/ARC/SiO_2/c-Si).

Reactive ion etching (RIE) was performed for transferring patterns in the photoresist film to the SiO2 KOH etch mask. A 100-nm-thick Si3N4 spacer was placed in between the confinement mask and c-Si wafer. The stack of c-Si wafer and confinement mask with spacer layers was filled with the 20% KOH solution before immersed in the etch bath with the same concentration for 310 s at 50 °C to fabricate an inverted nano-pyramid structure with double periodicity. The 50 °C temperature was found to be ideal in terms of etch rate; it was fast enough that complete nanopyramids are formed in less than 3 minutes, but not too fast that can cause them to collapse. Figure 8a shows a schematic of the experimental setup of the etch bath with the confinement mask. Optical photograph of the patterned C-Si is shown in Fig. 8b and the SEM images of the inverted nano-pyramid array with double periodicity are shown in 8c

The left SEM image shows clear circular boundaries where the transition occurs between the mass transfer limited region (outer circle) and the surface reaction limited region (inner circle). The right figure shows a magnified SEM image of the boundary. The fully developed inverted nanopyramid with apex is shown in left, and the base of pyramid not fully developed is shown in right. This pattern is consistent with etch depth profiles prediction shown in Fig. 6b.

Conclusions

We have demonstrated the use of a confinement mask to control etch depth gradient in nano-patterned c-Si. The gradient is achieved by restricting mass transfer of the etchant thereby slowing down etch rate at the desired regions. Periodicity of the gradient is set by controlling clearance gap profile of the mask which can be achieved with lithography. The experimental demonstration qualitatively agrees with our prediction of etch depth profile for a mask configuration. In future work, we will deploy the model to optimize the periodicity for light trapping enchancement.

In this work, we assume that hydrogen produced in etching reaction are dissolved in the liquid while in the experiment, we observe presence of hydrogen bubbles. These bubbles can potentially affect the uniformity of the etch profile by masking the c-Si surface[23,24] thereby slowing the reaction locally. However, that effect is found to be negligible at the experimental condition used in this study and therefore not included in the analysis. Should that effect become important in the future work, we would incorporate it in the model.

Acknowledgments

We thank Vinneeth Sasidharan for the SEM pictures of the post-interference-lithography-patterned c-Si in Fig. 1. This work is supported primarily by the National Science Foundation under Cooperative Agreement No. SNM-1635334.

ORCID

Kristianto Tjiptowidjojo https://orcid.org/0000-0002-0726-3431

References

1. Wood Mackenzie Power & Renewables and Solar Energy Industries Association. Solar market insight report 2018 year in review https://seia.org/research-resources/solar-market-insight-report-2018-year-review.
2. International Technology Roadmap for Photovoltaic. 2018 results, 2019 https://itrpv.vdma.org/.
3. H. R. Stuart and D. G. Hall, "Absorption enhancement in silicon-on-insulator waveguides using metal island films." *Appl. Phys. Lett.*, **69**, 2327 (1996).
4. S. L. Diedenhofen, O. T. A. Janssen, G. Grzela, E. P. A. M. Bakkers, and J. Gómez Rivas, "Strong geometrical dependence of the absorption of light in arrays of semiconductor nanowires." *ACS Nano*, **5**, 2316 (2011).
5. S. E. Han and G. Chen, "Optical absorption enhancement in silicon nanohole arrays for solar photovoltaics." *Nano Lett.*, **10**, 1012 (2010).
6. E. Yablonovitch, "Statistical ray optics." *JOSA*, **72**, 899 (1982).
7. V. E. Ferry, M. A. Verschuuren, H. B. T. Li, E. Verhagen, R. J. Walters, R. E. I. Schropp, H. A. Atwater, and A. Polman, "Light trapping in ultrathin plasmonic solar cells." *Opt. Express*, **18**, A237 (2010).
8. S. J. Han, S. Ghosh, O. K. Abudayyeh, B. R. Hoard, E. C. Culler, J. E. Bonilla, S. M. Han, and S. E. Han, "Symmetry-breaking nanostructures on crystalline silicon for enhanced light trapping in thin film solar cells." *Opt. Express*, **24**, A1586 (2016).
9. A. Mavrokefalos, S. E. Han, S. Yerci, M. S. Branham, and G. Chen, "Efficient light trapping in inverted nanopyramid thin crystalline silicon membranes for solar cell applications." *Nano Lett.*, **12**, 2792 (2012).
10. M. S. Branham, W.-C. Hsu, S. Yerci, J. Loomis, S. V. Boriskina, B. R. Hoard, S. E. Han, and G. Chen, "Silicon solar cells: 15.7% efficient 10-μm-thick crystalline silicon solar cells using periodic nanostructures (adv. mater. 13/2015)." *Adv. Mater.*, **27**, 2268 (2015).
11. Z. Yu, A. Raman, and S. Fan, "Fundamental limit of nanophotonic light trapping in solar cells." *Proceedings of the National Academy of Sciences*, **107**, 17491 (2010).
12. T. A. Savas, M. L. Schattenburg, J. M. Carter, and H. I. Smith, "Large-area achromatic interferometric lithography for 100 nm period gratings and grids." *Journal of Vacuum Science & Technology B: Microelectronics and Nanometer Structures Processing, Measurement, and Phenomena*, **14**, 4167 (1996).
13. A. Raub, A. Frauenglass, and S. R. J. Brueck, "Large area patterning using interferometric lithography." US8685628 (2014).
14. G. T. A. Kovacs, N. I. Maluf, and K. E. Petersen, "Bulk micromachining of silicon." *Proc. IEEE*, **86**, 1536 (1998).
15. H. Seidel, L. Csepregi, A. Heuberger, and H. Baumgärtel, "Anisotropic etching of crystalline silicon in alkaline solutions." *J. Electrochem. Soc.*, **137**, 3612 (1990).
16. S. Hassan, D. Lowell, M. Adewole, D. George, H. Zhang, and Y. Lin, "Extraordinary light-trapping enhancement in silicon solar cell patterned with graded photonic super-crystals." *Photonics* (Multidisciplinary Digital Publishing Institute) Vol. 4, p. 50 (2017).
17. H. Zhang et al., "Polarization-independent all-silicon dielectric metasurfaces in the terahertz regime." *Photonics Research*, **6**, 24 (2018).
18. R. Alkire and H. Deligiani, "The role of mass transport on anisotropic electrochemical pattern etching." *J. Electrochem. Soc.*, **135**, 1093 (1988).
19. C. B. Shin and D. J. Economou, "Effect of transport and reaction on the shape evolution of cavities during wet chemical etching." *J. Electrochem. Soc.*, **136**, 1997 (1989).
20. I. A. Shah, W. J. P. Van Enckevort, and E. Vlieg, "Absolute etch rates in alkaline etching of silicon (1 1 1)." *Sensors and Actuators A: Physical*, **164**, 154 (2010).
21. S. A. Roberts, D. R. Noble, E. M. Benner, and P. R. Schunk, "Multiphase hydrodynamic lubrication flow using a three-dimensional shell finite element model." *Computers & Fluids*, **87**, 12 (2013).
22. P. R. Schunk et al., *Goma 6.0. Technical Report, Sandia National Laboratories (SNL-NM), Albuquerque, NM (United States); 3M SAND2013-1844 456348* (2013).
23. E. D. Palik, O. J. Glembocki, I. Heard Jr, P. S. Burno, and L. Tenerz, "Etching roughness for (100) silicon surfaces in aqueous koh." *J. Appl. Phys.*, **70**, 3291 (1991).
24. M. S. Kulkarni and H. F. Erk, "Acid-based etching of silicon wafers: mass-transfer and kinetic effects." *J. Electrochem. Soc.*, **147**, 176 (2000).